actuators

MDPI

Article

Integrated Vehicle Controller for Path Tracking with Rollover Prevention of Autonomous Articulated Electric Vehicle Based on Model Predictive Control

Yonghwan Jeong

Department of Mechanical and Automotive Engineering, Seoul National University of Science and Technology, 232 Gongneung-ro, Nowon-gu, Seoul 01811, Republic of Korea; yh.jeong@seoultech.ac.kr; Tel.: +82-2-970-6322

Abstract: This paper presents an integrated controller for an autonomous articulated electric vehicle (AAEV) for path tracking and rollover prevention. The AAEV is vulnerable to rollover due to the characteristics of the articulated frame steering (AFS) mechanism, which shows improved maneuverability and agility but not front wheel steering. In addition, the ratio between height and track width is high, so the AAEV is prone to rolling over. Therefore, the proposed controller was designed to achieve the two goals, following the reference path and managing the velocity to improve the safety of the AAEV. Vehicle behavior was modeled by a kinematic model with actuation delay. A local linearization was used to improve the accuracy of the vehicle model and reduce the computational load. Reference states of the position and heading were determined to follow the reference path and prevent the rollover. A model predictive control (MPC)-based reference state tracker was designed to optimize the articulation angle rate and longitudinal acceleration commands. The simulation study was conducted to evaluate the proposed algorithm with a comparison of the base algorithms. The reference path for the simulation was an S-shaped path with discontinuous curvature. Simulation results showed that the proposed algorithm reduces the path tracking error and load-transfer ratio.

Keywords: autonomous articulated electric vehicle; path-tracking control; velocity control; rollover prevention; model predictive control

Citation: Jeong, Y. Integrated Vehicle Controller for Path Tracking with Rollover Prevention of Autonomous Articulated Electric Vehicle Based on Model Predictive Control. *Actuators* **2023**, *12*, 41. https://doi.org/10.3390/act12010041

Academic Editors: Jiageng Ruan and Jinglai Wu

Received: 17 November 2022
Revised: 5 January 2023
Accepted: 11 January 2023
Published: 12 January 2023

1. Introduction

The articulated frame steering (AFS) mechanism has been widely used in various fields which require high maneuverability and a small turning radius. Since the early 20th century, heavy equipment for use in large-scale construction began to develop rapidly [1]. Currently, more than 80 kinds of heavy equipment have been developed and used around the world. Among them, heavy equipment with articulated structures began to appear in the 1950s [2]. Particularly, AFS has been adopted to develop vehicles for construction, forestry [3], and mining [4]. The representative examples are buses, trucks, trams, wheel loaders, and tractors. Recently, the small articulated vehicle has emerged for special purposes in indoors and narrow spaces. To use the articulated vehicle in indoors, the powertrain has been changed from internal combustion engines to electric motors [5]. In addition, the electrification of vehicles has drawn attention as a solution to improve the sustainability of transportation [6]. Particularly, the electrification of commercial vehicles is the key issue to reducing the pollutants from road transportation [7]. This is because commercial vehicles have a longer operating time than passenger cars. As a result, the proportion of pollution caused by commercial vehicles is greater than that of passenger cars [8]. An example of an indoor application with electrification is the electric road sweeper to clean factories [9–12]. The history of the cleaning robot and road sweeper is provided in [9,10], respectively. To use the road sweeper in indoors, the sweeping range was analyzed by the kinematic model [11]. Particularly, the curbside sweeping case was considered to extend the cleaning coverage [12]. When the road sweeper is operated on a public road, a

diesel engine is the most common powertrain. However, an electric motor with a battery replaces the diesel engine to reduce carbon emissions when used indoors.

The typical structure of the articulated vehicle is shown in Figure 1. As shown in Figure 1, the articulated vehicle is composed of two bodies, which are connected by a pivot joint. A heading difference of two bodies is used to define an articulation angle, γ. Depending on the purpose and operational design domain (ODD) of the vehicle, the pivot joint is permanent or semi-permanent. In this study, the joint is the permanent articulation and named an articulation joint to emphasize its role. In the case of steering, the wheels can be steerable or non-steerable with articulation. In this study, the non-steerable wheels are used to provide the driving and braking torque. Thus, the steering is accomplished by AFS by articulating the front and rear bodies with respect to each other. For the actuation of the articulation joint, a hydraulic cylinder is used to control the articulation angle. For longitudinal motion, a driving motor is attached to the front axle and a pneumatic brake with electronic stability control (ESC) is used to provide the brake-by-wire function. The articulated vehicle can be operated by the autonomous driving system and is named an autonomous articulated electric vehicle (AAEV).

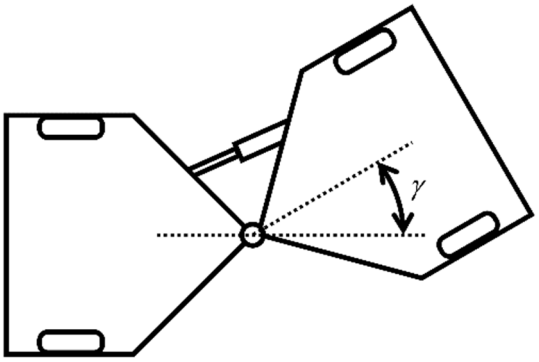

Figure 1. Structure of the articulated vehicle.

The characteristics of the AAEV can be summarized in three aspects. First, the AAEV shows improved maneuverability and agility to generate a larger lateral motion than front wheel steering (FWS) vehicles [13]. Particularly, oversteer and jack-knife motion were analyzed to provide the performance limit of the articulated vehicles [14]. From the analysis of the articulated vehicle, the AAEV has a smaller minimum radius of turning than a vehicle with FWS [15]. If the same articulation angle is applied with the front wheel steering angle, a larger yaw rate and lateral acceleration are generated by the AAEV than the FWS vehicle. The second aspect is that the operating velocity of the AAEV is limited to under 20 km/h. Therefore, the behavior of the AAEV can be represented by a kinematic model. The third aspect is that the height of the mass center is relatively higher than passenger cars', which means that the AAEV is prone to rollover. Therefore, the controller for the lateral and longitudinal motion to follow the reference path and prevent rollover is required.

Initially, the studies for the articulated vehicle focused on lateral stability. Similar to the analysis for FWS vehicles, the phase plane analysis was conducted by using CarSim to analyze the lateral stability of car-trailer combinations, which is one of the articulated vehicles [16]. The Hurwitz criterion was introduced to determine the approximation of the stability boundaries with a linear vehicle model [17]. Thus, the stability analysis can be made without nonlinear simulation software. A linear dynamic model with six degrees of freedom was also used to analyze the lateral stability [18]. Linear matrix inequalities were used to consider time-varying delay when analyzing the lateral stability [19]. In addition, the off-road condition was considered for stability analysis [20]. Based on the stability analysis, various controllers for lateral stability were proposed. For an articulated vehicle with FWS and with a passive articulation joint, such as a tractor and trailer, model predictive control (MPC) was used to determine the front steering input [21–23]. Active steering of the trailer was introduced to improve the stability of

the vehicle [21]. The additional lower-level controller was used to track the desired force and moment to stabilize the vehicle [22] and validated via experiment [23]. Various combinations of the actuators, such as differential braking [22], active steering of the trailer [21], or four-wheel independent driving [24], were considered to improve stability. Similarly, active rear-wheel steering of the tractor was introduced for lateral stability management using fuzzy logic and MPC [25]. Sliding mode control (SMC) was used to configure the robust controller for lateral stability [26–28]. Snaking stability was considered to prevent the oscillation of the high-speed driving condition [26]. An adaptive SMC [27] was utilized to improve the performance of the SMC. To deal with the nonlinear vehicle model, feedback linearization was used with dynamic SMC [28]. For an articulated vehicle with non-steerable wheels, snacking stability was analyzed to investigate the effect of the suspension [29].

The increased demand for the AFS-based vehicle leads to the automation of the driving task. Since an articulated vehicle requires different driving skills from that of a passenger vehicle, a lot of effort and time is required to train drivers. In addition, the articulated vehicle is commonly used for commercial purposes and has a considerable operating time. Therefore, research is being conducted by various researchers and companies to automate the driving task of the articulated vehicle. Since the AAEV has a different structure from a conventional vehicle, the autonomous driving system should be modified to optimize its performance. The key functions of autonomous driving are perception, localization, motion planning, and control [30]. As mentioned before, the ODD of the AAEV is restricted to the low-speed condition. Thus, the perception and localization can apply to the AAEV with minimal change to the algorithm. However, the different structures and dynamic behavior of the AAEV require a new design for motion planning and vehicle control. Generally, the AAEV is operated in a specific environment. In other words, the motion planner of the AAEV can be more simplified than that of the road vehicle. The key issue of the AAEV is to design a vehicle controller which is suitable for the AFS structure. Thus, this study focused on a control algorithm for the characteristics of the AAEV.

Based on the stability analysis and controller for lateral stability, various approaches have been proposed to design a path-tracking controller for articulated vehicles. For the articulated vehicle with a steerable wheel, similar approaches with the path tracking algorithm for FWS vehicles were proposed. The focus preview controller was proposed to follow the reference path by determining the steering angle of the tractor's front wheel. To enhance path tracking, the active steering controller for the trailer's wheel was designed based on a single-point preview model [31]. The combined controller of the kinematic model-based feed-forward controller and PID feedback controller was proposed to consider the low- and high-speed driving conditions [32]. Since the vehicle model for the articulated vehicle is nonlinear, backstepping was used to design a controller for an all-wheel-steered articulated vehicle [33]. The MPC was used to design a path tracker for the articulated vehicle. For highway conditions, the controller based on MPC was proposed to provide adaptive cruise control and trajectory tracking by modeling the electric tractor and trailer. The model for trajectory tracking was designed based on the preview control of the tractor [34]. The combined approach of the MPC-based path tracking and PID-based speed control was proposed to reduce the complexity of the vehicle model [35]. The lookup table and interpolation were introduced to improve the accuracy of the simple model by changing the parameters [36].

For articulated vehicles with non-steerable wheels, the path tracker is designed to determine the articulation angle to follow the path. A preview controller for the FWS vehicle is modified for the articulated vehicle [37]. A pure pursuit controller with a feedback controller was proposed. Since the geometric-based controller has the disadvantage of being vulnerable to position and heading errors, the heading predictor was used together with it to reduce the effect of the sensor noise [38]. The weighted PID controller was used to determine the articulation angle by using the weighted parameter, which is defined as a function of lateral and heading errors [39]. H-∞ control was used to determine the control gain systemically [40]. Since the vehicle model of the articulated vehicle is nonlinear,

backstepping [41] and feedback linearization [42] were utilized to design the path tracker. The MPC was used to improve the tracking performance. Multiple error dynamic models were used for MPC with a model switching rule to consider the slip angle under various driving conditions [43]. This study was extended to use full error dynamics [44]. Similarly, the MPC controller based on several fixed velocities was used to select the appropriate controller with respect to the driving velocity [45]. Nonlinear MPC (NMPC) was utilized to improve the path tracking performance in an environment where the accuracy of the linear model is degraded, such as low-speed driving [46].

Many approaches have been proposed to configure the path tracking controller for the articulated vehicle. Among the various types of articulated vehicles, the tractor-trailer was frequently considered a target platform [31–36]. Since the tractor has a steerable front wheel, the basic structure of the path tracker is similar to the FWS vehicle. Thus, the key issue of path tracking is to reflect the constraints arising from the trailer. The studies considering the articulated vehicle with non-steerable wheels focused on the design of the path tracker, which reflects the characteristics of the actuation of the articulation joint. Various linear and nonlinear models are derived to model the behavior of the articulated vehicle [41–46]. To consider the different behavior of the articulated vehicle, MPC has been used to configure the path tracker [43–46]. NMPC can directly consider the nonlinear vehicle model, but the computational burden increases significantly. Thus, the linear MPC-based approach is a method that can achieve real-time performance while comprehensively considering vehicle models, constraints, and actuator characteristics. For the AAEV, the rollover should be considered to secure safety when following the arbitrary path. However, many studies assumed the velocity of the vehicle is constant. If the target speed is set to high speed, the possibility of the rollover increases due to the separate architecture for the lateral and longitudinal control. Based on the lateral stability analysis of the articulated vehicle, the rollover should be considered when designing the controller. Therefore, it is necessary to design an integrated control algorithm for the AAEV to achieve path tracking and prevent rollover by controlling the articulation angle and longitudinal acceleration simultaneously.

The contributions of this paper are summarized as follows:

1. The proposed algorithm determines the control inputs for lateral and longitudinal motion simultaneously. Thus, the control moment for the AFS mechanism and front-wheel torque are determined to follow the reference path and improve the roll stability.
2. The proposed controller is designed to track the reference states, which can be calculated regardless of the road geometry. Therefore, the proposed approach can be applied to various kinds of roads.
3. The desired acceleration is derived to prevent the rollover by considering the lateral acceleration of the front and rear bodies of the AAEV. With the lateral acceleration threshold, an MPC-based controller determines the desired longitudinal acceleration for rollover prevention while considering the actuation delay.

The remains of this paper are organized as follows: Section 2 describes the overall architecture of the proposed algorithm. The vehicle model and state equation for the AAEV are derived in Section 3. The integrated controller for path tracking and velocity control is designed in Section 4. Section 4 consists of three subsections: reference state decision, MPC-based reference state tracker, and low-level controller. In Section 5, the simulation results are described to show the effectiveness of the proposed algorithm. The last section provides the conclusion and future works of this study.

2. Overall Architecture

The proposed algorithm is composed of three submodules with one external module. Figure 2 shows the overall architecture of the proposed controller for the AAEV. Vehicle sensors are used to measure the vehicle states, such as velocity, acceleration, and position. The external module, the reference path module, generates the global desired path for AAEV to reach the pre-defined destination. The path and vehicle information are used to determine the desired input for articulation and driving/braking actuators. The proposed

algorithm is designed based on the MPC to consider the future motion of the vehicle and constraints. First, a reference state decision module decides the reference position and heading angle of the AAEV. In addition, the maximum velocity to prevent the rollover of the AAEV is also determined when deciding the reference states. An MPC-based reference state tracker is designed to track the reference states while satisfying the constraints for state and input variables. The inputs are composed of the desired articulation angle rate and longitudinal acceleration of the front body. A low-level controller is used to generate the actuator inputs to follow the outputs of the MPC-based reference state tracker. In this study, the actuator inputs are the driving torque of the front axle, the total braking torque of the front and rear axles, and hydraulic cylinder pressure to control the articulation angle.

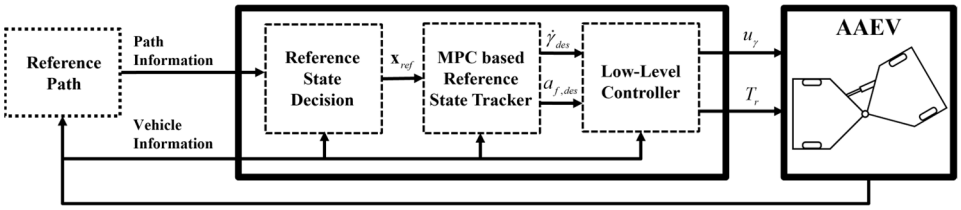

Figure 2. Overall architecture of the integrated control algorithm for the AAEV.

3. Articulated Vehicle Model

The articulated vehicle can be classified into two categories, vehicles with steerable wheels and vehicles with non-steerable wheels. As shown in Figure 1, the target platform of this study only has the AFS mechanism between the front and rear bodies to generate the yaw motion [41–46]. In other words, the AAEV has non-steerable wheels only. Thus, the articulation angle between the front and rear bodies due to the AFS mechanism can be considered the same as the steering angle of a typical front-wheel steering vehicle. Furthermore, under the assumption that the ODD is limited to a low-speed driving condition, the behavior of the AAEV can be represented by a kinematic bicycle model with an articulated frame [31,37–39,41–46]. In addition, the bicycle model effectively models the behavior of the AAEV from the validation results with the actual articulated vehicle data, which are given in [47]. The kinematic model for the AAEV is depicted in the global coordinate system as shown in Figure 3. Since the articulated vehicle has two relatively movable bodies, $P_f(x_f, y_f)$ and $P_r(x_r, y_r)$ are defined to represent the position of the center of the front and rear axles. To fully define the pose of each body, θ_f and θ_r are defined to represent the heading angle of the front and rear bodies with respect to the global coordinate system. Since the tire slip is negligible due to the low-speed driving [48], v_f and v_r are used to represent the velocities of each body. γ is the articulation angle between the front and rear bodies. L_f and L_r mean the distance from the articulation joint to the center of each axle.

The no-slip condition for each wheel is used to derive the kinematic model for the AAEV. As shown in Figure 3, the lateral velocity at each wheel is zero. In other words, the change rate of the $P_f(x_f, y_f)$ and $P_r(x_r, y_r)$ is the longitudinal velocity of each body. Therefore, the equation for the position of the front and rear body is defined as follows:

$$\begin{aligned} \dot{x}_f \sin\theta_f - \dot{y}_f \cos\theta_f &= 0 \\ \dot{x}_r \sin\theta_r - \dot{y}_r \cos\theta_r &= 0 \end{aligned} \tag{1}$$

Under low-speed driving conditions, the dynamic characteristics of the tire, friction, load, and braking forces are negligible. In addition, a large force is required to change the articulation angle. A hydraulic actuator is frequently used to provide sufficient force to control the articulation joint. This means that the actuator for articulation operates at a low speed. Generally, a digital controller has a sampling time of 10 to 100 ms. Therefore, it can be assumed that the articulation angle is considered constant during the sampling time of the controller under small displacements. Since the tire slip is negligible under low-

speed conditions, the changes of $P_f(x_f, y_f)$ and $P_r(x_r, y_r)$ are represented by the geometric relationships given in Figure 3.

$$\begin{cases} \dot{x}_f = v_f \cos\theta_f \\ \dot{y}_f = v_f \sin\theta_f \\ \dot{x}_r = v_r \cos\theta_r \\ \dot{y}_r = v_r \sin\theta_r \end{cases} \tag{2}$$

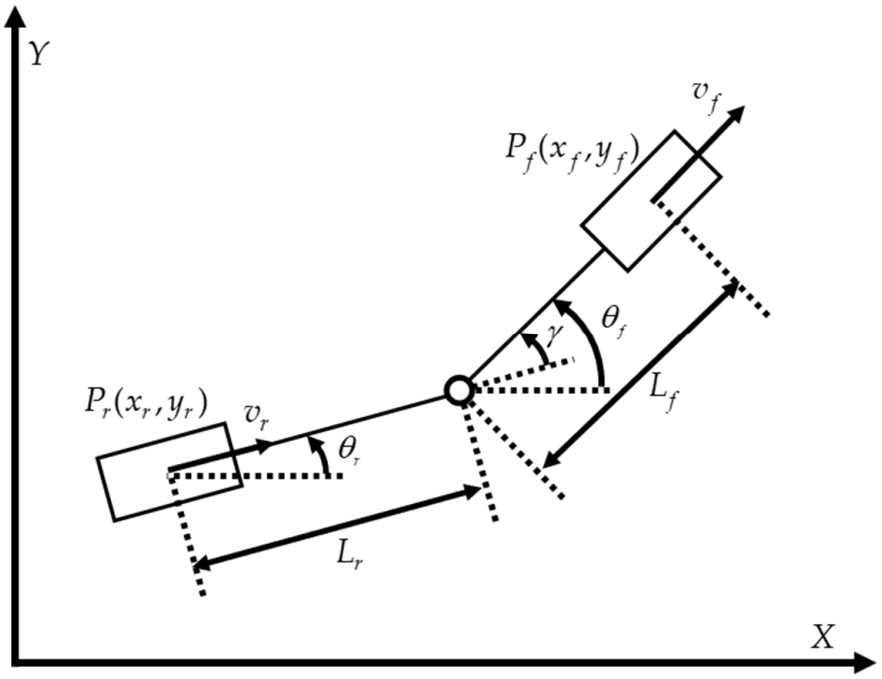

Figure 3. Kinematic model for the AAEV.

The front and rear bodies are connected by the rigid articulation joint. Therefore, the change rate of v_f and v_r is identical. v_f and v_r can be represented by other variables such as (3) and (4). In addition, the yaw rate of each body and articulation angle rate have the relationship seen in (5)

$$v_f = v_r \cos\gamma + \dot{\theta}_r L_r \sin\gamma \tag{3}$$

$$v_r = \dot{\theta}_f L_f \sin^{-1}\gamma + \dot{\theta}_r L_r \tan^{-1}\gamma \tag{4}$$

$$\dot{\theta}_r = \dot{\theta}_f - \dot{\gamma} \tag{5}$$

As given in (4), v_r can be obtained from the yaw rate of each body and articulation angle. To derive the yaw rate of the front body, (4) and (5) are substituted to (3) [48].

$$\dot{\theta}_f = \frac{v_f \sin\gamma + L_r\dot{\gamma}}{L_f \cos\gamma + L_r} \tag{6}$$

The actuation delay is considered to improve the accuracy of the vehicle model. The first-order delay model is introduced for the lateral and longitudinal actuators as given in (7). τ_γ and τ_a are the time delay for articulation and longitudinal actuator.

$$\begin{aligned} \ddot{\gamma} &= -\tfrac{1}{\tau_\gamma}\dot{\gamma} + \tfrac{1}{\tau_\gamma}\dot{\gamma}_{des} \\ \dot{a}_f &= -\tfrac{1}{\tau_a}a_f + \tfrac{1}{\tau_a}a_{f,des} \end{aligned} \tag{7}$$

The state and input vectors are defined as (8) and (9), respectively. The state vector is composed of seven states: position, heading, velocity and acceleration of the front body,

articulation angle, and rate. The input vector consists of $a_{f,des}$ and $\dot{\gamma}_{des}$. $a_{f,des}$ and $\dot{\gamma}_{des}$ are the desired acceleration of the front body and the desired articulation angle rate.

$$\mathbf{x} = \begin{bmatrix} x_f & y_f & \theta_f & v_f & a_f & \gamma & \dot{\gamma} \end{bmatrix}^T \tag{8}$$

$$\mathbf{u} = \begin{bmatrix} a_{f,des} & \dot{\gamma}_{des} \end{bmatrix}^T \tag{9}$$

The state equation of the kinematic model for AAEV is defined as (10) with state and input vectors. The behavior of the front body is defined by using (10). Since the front and rear bodies are connected by the rigid articulation joint, the position and heading angle of the rear body are calculated as (11).

$$\dot{\mathbf{x}} = \begin{bmatrix} v_f \cos\theta_f \\ v_f \sin\theta_f \\ \frac{v_f \sin\gamma}{L_f \cos\gamma + L_r} \\ a_f \\ -\frac{1}{\tau_a} a_f \\ \dot{\gamma} \\ -\frac{1}{\tau_\gamma} \dot{\gamma} \end{bmatrix} + \begin{bmatrix} 0 & 0 \\ 0 & 0 \\ 0 & \frac{L_r}{L_f \cos\gamma + L_r} \\ 0 & 0 \\ \frac{1}{\tau_a} & 0 \\ 0 & 0 \\ 0 & \frac{1}{\tau_\gamma} \end{bmatrix} \mathbf{u} = f(\mathbf{x}, \mathbf{u}) \tag{10}$$

$$\begin{cases} x_r = x_f - L_f \cos\theta_f - L_r \cos\theta_r \\ y_r = y_f - L_f \sin\theta_f - L_r \sin\theta_r \\ \theta_r = \theta_f - \gamma \end{cases} \tag{11}$$

4. Integrated Controller for Articulated Vehicle

The proposed controller for AAEV consists of three modules: reference state decision, MPC-based reference state tracker, and low-level controller. Since the proposed algorithm is designed to determine the lateral and longitudinal motion simultaneously, the reference state decision includes not only the reference states but also the constraints to prevent the rollover of the AAEV. The MPC approach is used to track the reference state while satisfying the constraints and considering the actuation delay. The MPC-based tracker determines the desired articulation angle rate and acceleration of the front body. The low-level controller is used to determine the actuator inputs to follow the desired values from the MPC-based tracker. The details of the proposed integrated controller for the AAEV are described in the following subsections.

4.1. Reference State Decision

Conventional approaches have used the position error with respect to the reference path to determine the control input. Pure pursuit and Stanley methods are representative examples of path tracking using position errors. However, it is difficult to design the integrated controller for lateral and longitudinal motion by using an error-based approach. This is because there are difficulties in the gain tuning of feedback controllers for lateral and longitudinal errors. If a model-based controller is used, the model complexity increases excessively to consider the lateral and longitudinal motion simultaneously. In addition, considering the constraints and actuator dynamics increase the complexity of the controller. Furthermore, an error dynamics-based approach uses the time derivative of the errors. To define the time derivative of the error, the reference path should be designed as a differentiable form. In this study, the path tracking and velocity controller was separated into two independent modules, reference state decision and reference state tracker to overcome the limitations of the previous approaches. Thus, the decision of the reference state can be determined independently by the controller.

The reference states for the AAEV are determined to follow the reference path and prevent the rollover of both bodies. The reference state decision module utilizes the geometric relationships between the AAEV and reference path [47,49]. The first step of the

reference state decision is defining the desired path. Figure 4 shows a graphical description of the desired path decision. To avoid the singularity of the curve fitting, the waypoints of the reference path are converted to the local coordinate system of the AAEV. The origin of the local coordinate system is located in the articulation joint and the x-axis heads from the rear axle center to the articulation joint. Since the length of the vehicle is short and the articulation angle has a constraint on the maximum angle, the local coordinate system on the articulation joint can prevent the singularity of the curve fitting. The nearest point from the articulation joint is searched on the reference path as shown in Figure 4. The point ahead by the preview distance from the nearest point along the reference path is set as the preview point, which is marked as a yellow circle. The preview distance is calculated as proportional to the vehicle speed. The proportional gain K is set as constant because the driving condition of the AAEV is limited to low-speed situations. Then, the preview points for front and near bodies are selected in front L_f and behind L_r of the preview point of the articulation joint. In previous studies, a geometric relationship with the road was derived based on one side of the articulated vehicle, even though the vehicle body can be articulated. To consider the stability of the articulated vehicle, this study derived the desired path for both bodies. The preview points for each body are represented as red and blue circles, respectively.

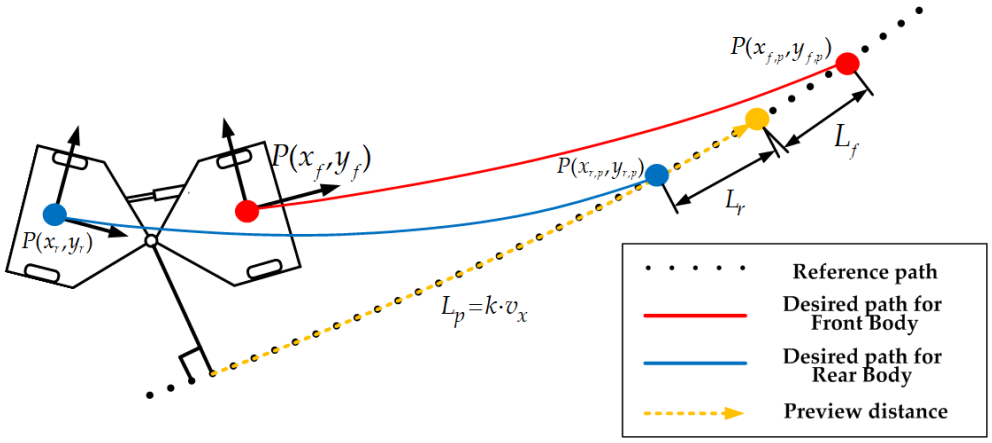

Figure 4. Desired path for both bodies of the AAEV.

The desired path is defined to connect the axle centers of each body and the preview points. The desired path is designed as a second-order polynomial as given in (12) in the local coordinate system of the AAEV. Since the purpose of the desired path is to provide the reference state for MPC, which optimizes the states and inputs, second-order polynomial is appropriate to guide the vehicle toward the reference path.

$$y_i(x) = a_{i,2}{x_i}^2 + a_{i,1}x_i + a_{i,0}, \quad i = f, r \tag{12}$$

Three constraints are required to fully define the desired path. The position of the axle centers and the preview points are used to define the two constraints. Since the body slip is assumed to be zero, the heading of the desired path at the axle centers should be aligned with the heading of each body. Thus, the coefficient of (12) is calculated from the position constraints on $P(x_i, y_i)$ and $P(x_{i,p}, y_{i,p})$, and heading constraints on $P(x_i, y_i)$.

$$\begin{bmatrix} a_{i,2} \\ a_{i,1} \\ a_{i,0} \end{bmatrix} = \begin{bmatrix} {x_i}^2 & x_i & 1 \\ {x_{i,p}}^2 & x_{i,p} & 1 \\ 2x_i & 1 & 0 \end{bmatrix} \begin{bmatrix} y_i \\ y_{i,p} \\ y_i'(x_i) \end{bmatrix}, \quad i = f, r \tag{13}$$

After the desired path is determined, a curvature κ_{ref} at $P(x_i, y_i)$ is calculated to derive the reference motion and articulation angle rate. The κ_{ref} is calculated as follows:

$$\kappa_{i,des} = \frac{y_i''(x_i)}{\sqrt{\left(1 + y_i'(x_i)^2\right)^3}},\ i = f, r \tag{14}$$

The reference yaw rate of each body is derived from the κ_{ref} and velocity as (15). The reference velocity of each body should be determined to prevent the rollover of the AAEV and follow the reference path simultaneously. The reference velocity is determined so that the AAEV does not exceed the lateral acceleration threshold, $a_{y,th}$ [50,51]. Since the AAEV should follow the reference path while maintaining the path deviation within a reasonable level, the reference velocity should be reduced as given in (16).

$$\dot{\theta}_{i,ref} = k_{i,ref} \cdot v_i, \quad i = f, r \tag{15}$$

$$v_{i,ref} = \min\left(v_{set},\ \sqrt{\frac{a_{y,th}}{\dot{\theta}_{i,ref}}}\right),\ i = f, r \tag{16}$$

The $v_{i,ref}$ will be used as a velocity constraint of the MPC-based reference state tracker. If the yaw rate of the AAEV is matched to the reference one as given in (15), the AAEV drives toward the reference path and follows it. Thus, the reference articulation angle rate $\dot{\gamma}_{ref}$ can be calculated by using (6) in Section 3.

$$\dot{\gamma}_{ref} = \frac{1}{L_r}\left\{\dot{\theta}_{f,ref}\left(L_f \cos\gamma + L_r\right) - v_f \sin\gamma\right\} \tag{17}$$

Based on the $v_{i,ref}$ and $\dot{\gamma}_{ref}$, the reference states are determined by integrating the vehicle model for the AAEV. The purpose of the reference state decision is to provide the optimal reference motion for path tracking. Therefore, the actuator delay is not considered. The equation for the integration of the $v_{i,ref}$ and $\dot{\gamma}_{ref}$ is derived as (18). In Section 3, the state vector of the vehicle model is composed of seven elements. In the previous studies which use the MPC, the reference state has the same number of the element as the plant model. However, this study only defines the reference state for the position and heading of the front body to increase the degree of freedom in the process of optimizing control inputs. If the reference for γ or $\dot{\gamma}$ is defined, the MPC controller only finds the actuator inputs derived from the vehicle model because the vehicle model already includes the equation for γ. This undermines the advantages of the MPC. Thus, the v_f, a_f, γ, and $\dot{\gamma}$ are excluded from the reference state decision. The derivative of the position and heading angle of the front body from (18) is integrated as (19) with a discrete-time index k and ΔT, the sampling time of the MPC.

$$\begin{aligned}
\dot{x}_f(k) &= v_{ref}(k)\cos\theta_f(k) \\
\dot{y}_f(k) &= v_{ref}(k)\sin\theta_f(k) \\
\dot{\theta}_f(k) &= \tfrac{\sin\gamma(k)}{L_f\cos\gamma(k)+L_r} v_{ref}(k) + \tfrac{L_r}{L_f\cos\gamma(k)+L_r}\dot{\gamma}_{ref}(k)
\end{aligned} \tag{18}$$

$$\begin{bmatrix} x_f(k) \\ y_f(k) \\ \theta_f(k) \end{bmatrix} = \begin{bmatrix} x_f(k-1) \\ y_f(k-1) \\ \theta_f(k-1) \end{bmatrix} + \begin{bmatrix} \dot{x}_f(k) \\ \dot{y}_f(k) \\ \dot{\theta}_f(k) \end{bmatrix} \Delta T \tag{19}$$

4.2. MPC-Based Reference State Tracker

The MPC problem is composed of a cost function and constraints. To define the cost function, the type of MPC should be determined first. In Section 3, the vehicle model is derived as a nonlinear system as given in (10). Thus, a solver for an NMPC should be

introduced to optimize the control input while considering the nonlinear plant model, constraints, and cost function. However, the NMPC requires a larger computational load than a linear MPC to determine the control inputs. Even if the solution from NMPC is more accurate than linear MPC, the increased sampling time of the controller degrades the control performance. Therefore, this study uses the linear MPC to design the reference state tracker. The cost function is defined as a linear quadratic form to follow the reference state and minimize the control efforts.

$$J = \sum_{k=1}^{T_p/\Delta T} \left[\widetilde{\mathbf{x}}_{ref}(k)^T \mathbf{Q} \widetilde{\mathbf{x}}_{ref}(k) + \mathbf{u}(k)^T \mathbf{R} \mathbf{u}(k) \right] + \rho \varepsilon \tag{20}$$

where $\widetilde{\mathbf{x}}_{ref}$ is the reference state tracking error, which is defined as follows:

$$\begin{aligned} \widetilde{\mathbf{x}}(k)(k) &= \mathbf{x}(k) - \mathbf{x}_{ref}(k) \\ &= \begin{bmatrix} x_f(k) \\ y_f(k) \\ \theta_f(k) \end{bmatrix} - \begin{bmatrix} x_{f,ref}(k) \\ y_{f,ref}(k) \\ \theta_{f,ref}(k) \end{bmatrix} \end{aligned} \tag{21}$$

T_p and ΔT are the prediction horizon and sampling time of the MPC. Thus, the maximum prediction step is defined by dividing T_p by ΔT. The slack variable ε is used in the cost function to improve the convergence of the optimization. If the slack variable is not used in MPC formulation, the MPC has a possibility of failure to find the optimal solution. In this case, another backup controller is required to avoid this risky situation. However, the multiple controllers increase the complexity of the algorithm. Since the purpose of the proposed controller is path tracking and rollover prevention, longitudinal acceleration has a lower priority than other issues. For this reason, the ε is introduced to the cost function and the constraint for the acceleration inputs [52]. If the MPC could not find the optimal solution satisfying the constraints, the ε releases the constraint for the acceleration input to find the suboptimal solution with the minimum violation. The details of the constraints will be presented at the end of this subsection. The weight factor ρ is used to control the effect of ε. $\mathbf{Q}$ and $\mathbf{R}$, which are defined as (22), are the weight matrices for the reference tracking and control input effort, respectively.

$$\mathbf{Q} = \begin{bmatrix} Q_x & & \\ & Q_y & \\ & & Q_\theta \end{bmatrix}, \ \mathbf{R} = \begin{bmatrix} R_a & \\ & R_\gamma \end{bmatrix} \tag{22}$$

Q_x, Q_y, and Q_θ are the weights for the tracking error of x_f, $y_{f,}$ and θ_f, respectively. R_a and R_γ are the weights for the acceleration and articulation angle rate inputs.

The constraints of the proposed algorithm can be classified into two categories: equality and inequality constraints. The equality constraints are composed of the initial and dynamic constraints. Since the proposed algorithm is designed in the local coordinate system, the initial condition $\mathbf{x}(1)$ is all zeros. The vehicle model is used as a dynamic constraint. This study introduces local linearization to linearize the vehicle model at the current state of the AAEV. Since the driving condition of the AAEV is in the low-speed range, the prediction horizon covers the limited region from the current states. Thus, a time-varying linearized model can represent the behavior of the AAEV. The vehicle model given in (10) is linearized as (23) with the $\mathbf{x}(t)$ and $\mathbf{u}(t-1)$.

$$\begin{aligned} \dot{\mathbf{x}}(t) &= \mathbf{A}(t)\mathbf{x}(t) + \mathbf{B}(t)\mathbf{u}(t) \\ &= \left(\frac{\partial f(\mathbf{x},\mathbf{u})}{\partial \mathbf{x}} \Big|_{\mathbf{x}(t),\mathbf{u}(t-1)} \right) \mathbf{x}(t) + \left(\frac{\partial f(\mathbf{x},\mathbf{u})}{\partial \mathbf{u}} \Big|_{\mathbf{x}(t),\mathbf{u}(t-1)} \right) \mathbf{u}(t) \end{aligned} \tag{23}$$

$\mathbf{A}(t)$ and $\mathbf{B}(t)$ are defined as follows:

$$\mathbf{A}(t) = \begin{bmatrix} 0 & 0 & a_{13} & a_{14} & 0 & 0 & 0 \\ 0 & 0 & a_{23} & a_{24} & 0 & 0 & 0 \\ 0 & 0 & 0 & a_{34} & 0 & a_{36} & a_{37} \\ 0 & 0 & 0 & 0 & a_{45} & 0 & 0 \\ 0 & 0 & 0 & 0 & a_{55} & 0 & 0 \\ 0 & 0 & 0 & 0 & 0 & 0 & a_{67} \\ 0 & 0 & 0 & 0 & 0 & 0 & a_{77} \end{bmatrix}$$
$$a_{13} = -v_f \sin(\theta_f),\ a_{23} = v_f \cos(\theta_f)$$
$$a_{14} = \cos(\theta_f),\ a_{24} = \sin(\theta_f),\ a_{34} = \frac{\sin(\gamma)}{L_f \cos(\gamma) + L_r}$$
$$a_{45} = 1,\ a_{55} = -\frac{1}{\tau_a}$$
$$a_{36} = \frac{v_f \cos(\gamma)}{L_f \cos(\gamma) + L_r} + \frac{L_f \sin(\gamma) \cdot \left(L_r \dot{\gamma} + v_f \sin(\gamma)\right)}{\left(L_f \cos(\gamma) + L_r\right)^2}$$
$$a_{37} = \frac{L_r}{L_f \cos(\gamma) + L_r},\ a_{67} = 1,\ a_{77} = -\frac{1}{\tau_\gamma} \tag{24}$$

$$\mathbf{B}(t) = \begin{bmatrix} 0 & 0 \\ 0 & 0 \\ 0 & 0 \\ 0 & 0 \\ \frac{1}{\tau_a} & 0 \\ 0 & 0 \\ 0 & \frac{1}{\tau_\gamma} \end{bmatrix} \tag{25}$$

To apply the linearized state equation to discrete-time MPC, Equation (23) is discretized as (26) by using the first-order difference.

$$\begin{aligned} &\mathbf{x}(k+1) = \mathbf{A}_d(k)\mathbf{x}(k) + \mathbf{B}_d(k)\mathbf{u}(k) \\ &\textit{where} \quad \mathbf{A}_d(k) = \mathbf{I} + \mathbf{A}(t)\Delta T \\ &\qquad\quad \mathbf{B}_d(k) = \mathbf{B}(t)\Delta T \end{aligned} \tag{26}$$

The discretized linear time-varying model in (26) is used to define the dynamic constraints as follows:

$$\begin{aligned} \mathbf{x}(2) &= \mathbf{A}_d(1)\mathbf{x}(1) + \mathbf{B}_d(1)\mathbf{u}(1) \\ &\vdots \\ \mathbf{x}(N_p) &= \mathbf{A}_d(N_p - 1)\mathbf{x}(N_p - 1) + \mathbf{B}_d(N_p - 1)\mathbf{u}(N_p - 1) \end{aligned} \tag{27}$$

The inequality constraints are defined for the state and input vectors to regulate the vehicle motion within the design boundaries. For the state vector, the constraints for the velocity and acceleration are defined as follows:

$$v_{\min} < v_i(k) < v_{i,ref}(k),\ i = f, r \tag{28}$$

$$a_{x,\min} < a_f(k) < a_{x,\max} \tag{29}$$

$$-\gamma_{\max} < \gamma(k) < \gamma_{\max} \tag{30}$$

The constraints of $v_i(k)$ are defined to regulate the maximum lateral acceleration under the threshold. Thus, the reference velocity $v_{i,ref}(k)$, which is calculated to maintain the lateral acceleration under the threshold, is used to define the upper boundary of $v_i(k)$. The constraint of $v_r(k)$ is derived from the state vector and (4). In addition, the front and rear

bodies are rigidly connected by the articulation joint. Thus, the acceleration constraint is only defined for the front body. The constraints for the input vector are defined as follows:

$$\begin{array}{c} a_{x,\min} < a_{f,des}(k) < a_{x,\max} \\ -\dot{a}_{x,\max} < \dot{a}_{f,des}(k) < \dot{a}_{x,\max} \end{array} \tag{31}$$

$$\begin{array}{c} -\dot{\gamma}_{\max} < \dot{\gamma}_{des}(k) < \dot{\gamma}_{\max} \\ -\ddot{\gamma}_{\max} < \ddot{\gamma}_{des}(k) < \ddot{\gamma}_{\max} \end{array} \tag{32}$$

where $a_{x,\mathrm{mix}}$, and $a_{x,\max}$ are the minimum and maximum longitudinal acceleration. $\dot{a}_{x,max}$ is the maximum longitudinal jerk. $\dot{\gamma}_{max}$ and $\ddot{\gamma}_{max}$ are the maximum angular rate and acceleration of the articulation actuator. Thresholds for the input vector are designed to control the AAEV smoothly. In other words, the thresholds for the actuator for the longitudinal motion and articulation are set to smaller values than the actuator limits. Table 1 summarizes the values of the parameters for the AAEV and MPC-based reference state tracker.

Table 1. Parameters for AAEV and MPC-based reference state tracker.

Parameter	Value	Parameter	Value
L_f	0.8 m	ΔT	0.1 s
L_r	1.0 m	N_p	20
Q_x	1	R_a	1
Q_y	15	$v_{\min}$	0 m/s
Q_θ	20	$\gamma_{\max}$	30 deg
$R_{\dot{\gamma}}$	10	$\dot{\gamma}_{\max}$	30 deg/s
$a_{x,\min}$	-3 m/s^2	$\ddot{\gamma}_{\max}$	30 deg/s^2
$a_{x,\max}$	1 m/s^2	$\dot{a}_{x,\max}$	10 m/s^3

4.3. Low-Level Controller

The MPC-based reference state tracker determines the desired longitudinal acceleration and articulation angle rate to follow the reference path while managing the lateral acceleration. Given the desired values, the actuator input should be determined for the AAEV to generate the desired motion. For steering, the actuator inputs for the articulation joint should be determined to generate the steering moment to follow the desired articulation angle. For longitudinal motion, the driving and braking torque of the wheel is generated by the electric motor and electromagnetic brake (EMB). Thus, the inputs for the motor and EMB should be determined to follow the desired longitudinal acceleration. Therefore, the low-level controller is proposed to follow the desired inputs.

The actuator of the AAEV can be changed based on the vehicle configuration. Thus, the low-level controller is designed by the PID controller to determine the actuator inputs from the tracking errors. The articulation actuator input is calculated by the PID controller using the error between $\dot{\gamma}$ and $\dot{\gamma}_{des}$. In this study, the articulation actuator input is assumed to be hydraulic cylinder pressure. For longitudinal motion, the error between a_f and $a_{f,des}$ is used to determine the driving/braking torque of the wheels. The low-level controller for the AAEV is designed as (33). u_γ and u_a are the control input for the articulation actuator and torque of the wheels, respectively. If u_a is a positive value, the input is used to drive the front wheel. Meanwhile, if u_a is a negative value, the input is distributed to the front and rear axles by using the proportioning valve. The reference of the low-level controller, the output of the MPC, is determined by considering the constraints for the vehicle states and control inputs. Thus, the u_γ and u_a can be used to control the vehicle without a drastic change in the behavior of the AAEV.

$$\begin{array}{c} u_\gamma = K_{ps}e_\gamma + K_{is}\int e_\gamma dt + K_{ds}\dot{e}_\gamma,\ e_\gamma = \dot{\gamma}_{des} - \dot{\gamma} \\ u_a = K_{pa}e_a + K_{ia}\int e_a dt + K_{da}\dot{e}_a,\ e_a = a_{f,des} - a_f \end{array} \tag{33}$$

5. Simulation Results

The simulation study was conducted to evaluate the effectiveness of the proposed algorithm. Four base algorithms were used to compare the performance with the proposed algorithm. The details of the base algorithms are described in the following section. MATLAB/Simulink was used to configure the simulation environments. Thus, the reference decision module and low-level controller were implemented by using MATLAB/Simulink. The MPC-based reference state tracker was implemented by CVXGEN, which is a solver for a convex optimization problem. The problem should be a quadratic program representable to use the CVXGEN [53].

5.1. Vehicle Model for Simulation

The vehicle model is required to conduct the closed-loop simulation for the vehicle controller. Since the commercial vehicle simulation software does not include the articulated vehicle, this study uses the nonlinear dynamic bicycle model for the AAEV. The free-body diagram of the vehicle model for simulation is depicted in Figure 5. The equation of motion for each body is derived to model the behavior of the AAEV. When deriving the equation of the motion, the joint is assumed to apply the steering moment of the articulated frame. The dynamics of the articulation actuator are modeled as a second-order system to consider the torsional stiffness and damping. The STI (System Technology Inc., Joliet, IL, USA) tire model is used to calculate the longitudinal and lateral tire force of the front and rear wheels. The wheel dynamics is used to obtain the longitudinal tire force from the driving/braking torque of the wheel, which is determined by (33). Thus, the vehicle model for simulation is more accurate than the kinematic model for the MPC formulation. In other words, a different vehicle model is used for the MPC-based controller and simulation model to improve the reliability of the simulation study. The details of the accuracy analysis of the vehicle model for simulation with vehicle test results are provided in [47].

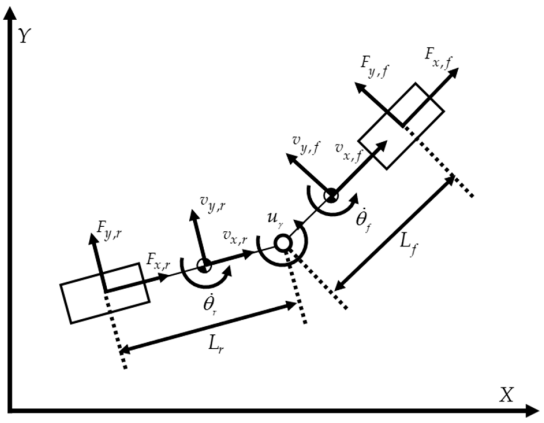

Figure 5. Free body diagram of the AAEV.

5.2. Base Algorithm

Three base algorithms were designed separately for lateral and longitudinal motion. For lateral motion, the conventional path tracking controller, pure pursuit, and Stanley methods are used to determine the desired articulation angle. Pure pursuit and Stanley methods are the representative path tracking controller for FWS vehicles. The articulation mechanism is considered to be front steering to apply the path tracking controller for the FWS vehicle to the AAEV. Thus, the position of the rear axle center and the entire wheelbase by adding L_f and L_r are used to calculate the desired articulation angle. The details of the pure pursuit and Stanley methods are described in [54,55]. The conventional path tracking algorithm requires the vehicle model to derive the controller. However, the unique structure of the AAEV makes it difficult to derive the model-based path tracker. A model-free approach is introduced to design the path tracker without a vehicle model [49]. The model-free method is defined by integrating the preview controller and lateral dynamics

based on the first-order delay model. The simplified lateral dynamics is defined as a first-order transfer function between steering angle δ and yaw rate $\dot{\theta}$ as (34).

$$\dot{\theta} = \frac{\lambda}{\tau s + 1}\delta \tag{34}$$

where τ and λ are the yaw rate delay and yaw rate gain, respectively. The preview model determines the desired yaw rate to follow the reference path. Thus, if λ is automatically adjusted to match the actual relationship between δ and $\dot{\theta}$, the steering angle to generate the desired yaw rate can be obtained by (34). The adaptation law for λ is defined as follows:

$$\hat{\lambda} = -k \cdot \delta \cdot \left(\dot{\theta}_{des} - \dot{\theta}\right) \tag{35}$$

where k is adaptation gain. Then, the steering angle, which is used as an articulation angle input, is determined as (36).

$$\delta = \frac{1}{\hat{\lambda}}\left(\dot{\theta}_{des} + \tau \cdot \ddot{\theta}_{des}\right) \tag{36}$$

The desired yaw rate $\dot{\theta}_{des}$ is obtained by the same method given in Section 4.1. Among the two $\dot{\theta}_{des}$, the value from the rear body is used for the model-free method.

To determine the speed of the AAEV, a longitudinal controller is designed for the pure pursuit, Stanley, and model-free method. As mentioned before, the lateral controller uses a single reference point to determine the steering angle. This reference point is also used to determine the desired velocity of the base algorithms. The curvature at the reference point is used to determine the safe velocity to manage the lateral acceleration of the AAEV. The same equation of (16) is used to determine the desired velocity. The reference point of the pure pursuit and model-free methods is a preview point. The Stanley method uses the closest point as a reference point.

The MPC approach is used to design another base algorithm. The base algorithm using MPC is the integrated controller to determine the steering input and desired velocity, simultaneously. The MPC-based base algorithm uses a simplified model of the AAEV, which only considers the behavior of the front body. The desired velocity is used as a reference state to manage the lateral acceleration and rollover. Thus, the desired velocity is utilized as one of the terms of the cost function. The details of the MPC-based base algorithm are described in [47]. In addition, NMPC based on the AAEV model for the simulation is configured to provide the reference for the performance comparison. Since the NMPC uses the same model as the simulation environment, it is possible to show the optimal performance. Furthermore, the vehicle model in the simulation utilizes a nonlinear tire model, which is more accurate than the kinematic model to show the behavior of the severe maneuver. The NMPC is implemented by using the CasADi solver [56].

5.3. Simulation Results

To evaluate the proposed algorithm, the S-shaped path is used as a reference path. The S-shaped path is designed by connecting the two straight lines and arcs with three junction points. Thus, the road curvature at the junction points changes discontinuously. Particularly, the sign of the road curvature is changed at the junction point between two arcs, so that the curvature change is maximized. A severe change in road curvature not only causes the discontinuity of the control input, but also increases the possibility of rollover due to the sudden change of the input. For longitudinal motion, the set speed v_{set} was set to 4 m/s, which is fast enough to cause the rollover on the S-shaped path. Therefore, if the appropriate control for longitudinal motion is not provided, the AAEV will roll over during the path following. From the analysis results of the AAEV, the AAEV will roll over with an LTR of 1 at about 3.0 m/s with the driving condition under the maximum articulation angle [56]. In this case, the lateral acceleration is about 3.25 m/s^2. To consider the effect of

the transition of the articulation and safety factor, the lateral acceleration threshold, $a_{y,th}$, is set to 1.0 m/s^2 for rollover prevention.

To measure the rollover propensity of a vehicle, the load transfer ratio (LTR) is adopted as an index to express the risk of rollover. The critical angle of the rollover is also one of the indexes for determining the rollover of the vehicle. However, since the critical changes depend on the specifications and loadings of the AAEV, the LTR, which is derived from the vertical tire force of each wheel, was used instead in this study. For a unibody vehicle, LTR is defined as the ratio of the difference in the load between the left and right wheels to the entire load on all wheels. However, the AAEV is composed of two bodies, which have different dynamic behavior and loads. If one of the bodies rolls over, the entire vehicle rolls over. Therefore, the LTR should be considered for each of the two bodies separately as given in (37). If one of the LTRs is equal to one, it can be said that the vehicle is under rollover.

$$\mathrm{LTR}_i = \frac{|F_{zi,L} - F_{zi,R}|}{F_{zi,L} + F_{zi,R}},\ i = f, r \tag{37}$$

The simulation results for the S-shaped path with a radius of 4 m are depicted in Figures 6 and 7. The road friction coefficient is set to 0.85 to generate lateral force enough to cause the vehicle to roll over. Table 2 summarizes the key performance index of the simulation. The mean, standard deviation (SD), and a maximum of the lateral and heading errors are summarized in Table 2. In addition, the maximum of the a_y and LTR are also presented in Table 2.

Figure 6 shows the reference path and driving trajectories of the base and proposed algorithms. The trajectory of the (x_f, y_f) is represented in Figure 6. Since the velocity control is applied for all algorithms, the AAEV follows the reference path regardless of the path tracking controller. However, the trajectory of each algorithm shows different behavior. The trajectory of the pure pursuit method, which is marked as a green dash-dotted line, did not follow the reference path and went out to the outside of the corner. This result means that the pure pursuit method is vulnerable to actuation delay. The Stanley method, which is presented as a magenta dashed line, shows a better performance than the pure pursuit method. However, after passing the first arc, the AAEV drove inside the reference path. This phenomenon is a typical feature of a steering control method using preview control using a single preview point. In other words, the path tracker based on the single preview point has a weakness to respond to discontinuous changes in curvature. A similar phenomenon also occurred for the model-free method and MPC controller, which are marked as a blue dotted line and a cyan solid line, respectively. Thus, all trajectories of the base algorithms have a large position and heading error near the inflection point of the reference path. However, the trajectory of the proposed algorithm and NMPC, which are depicted as a red dashed line and blue solid line, shows the most similar shape to the reference path. In other words, the position and heading errors of the proposed algorithm and NMPC were maintained at the smallest value among the base algorithms in all sections of the reference path. In particular, the control performance at the inflection point has been significantly improved compared to the base algorithms. Thus, it can be said that the proposed algorithm improves the path tracking performance in severe driving conditions and achieve the almost same performance as NMPC.

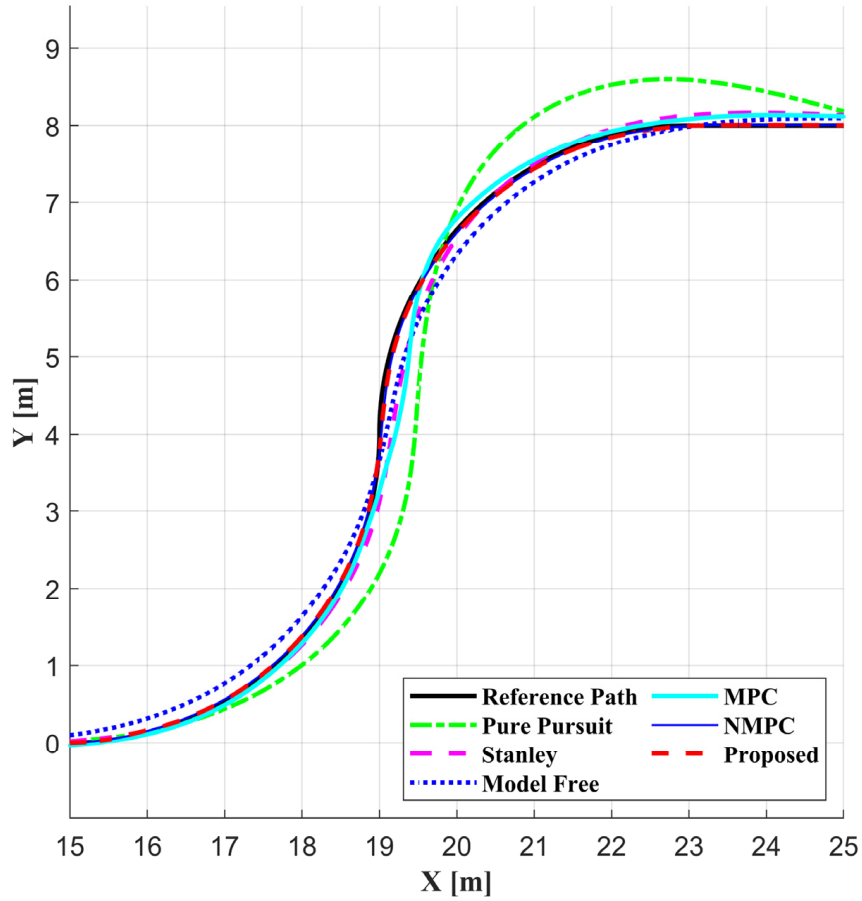

Figure 6. Driving trajectories of each algorithm.

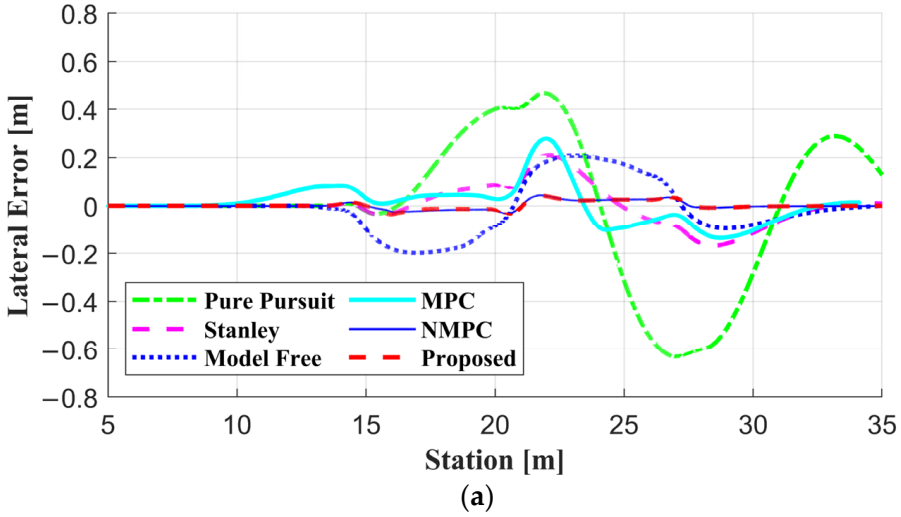

(**a**)

Figure 7. *Cont.*

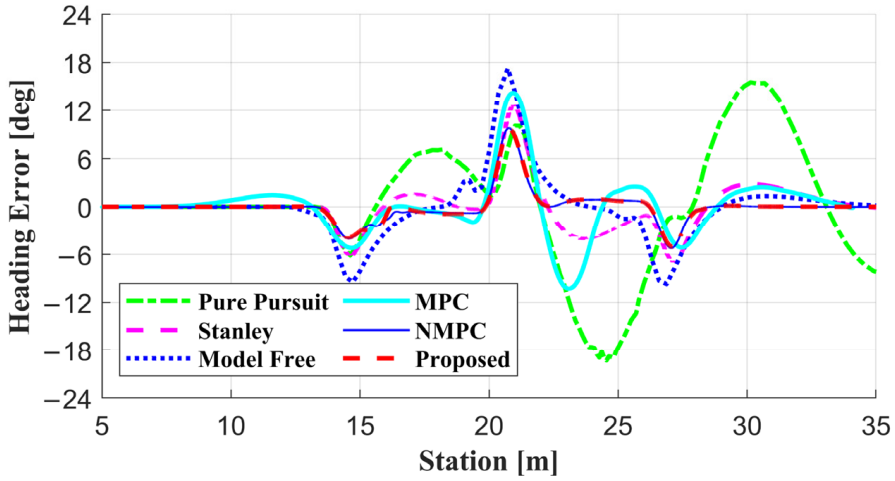

(**b**)

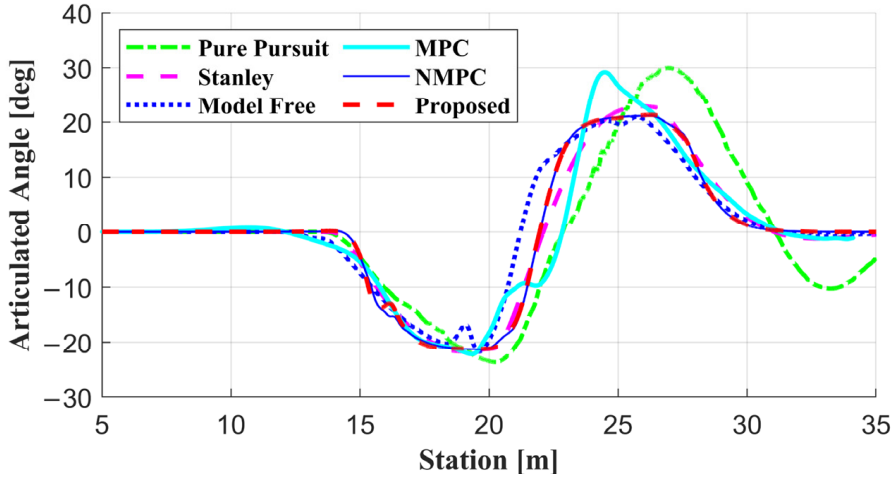

(**c**)

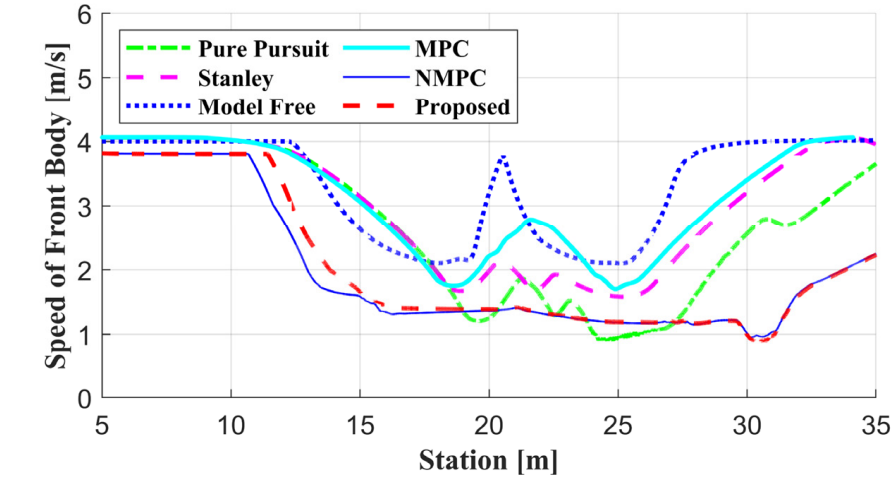

(**d**)

Figure 7. *Cont.*

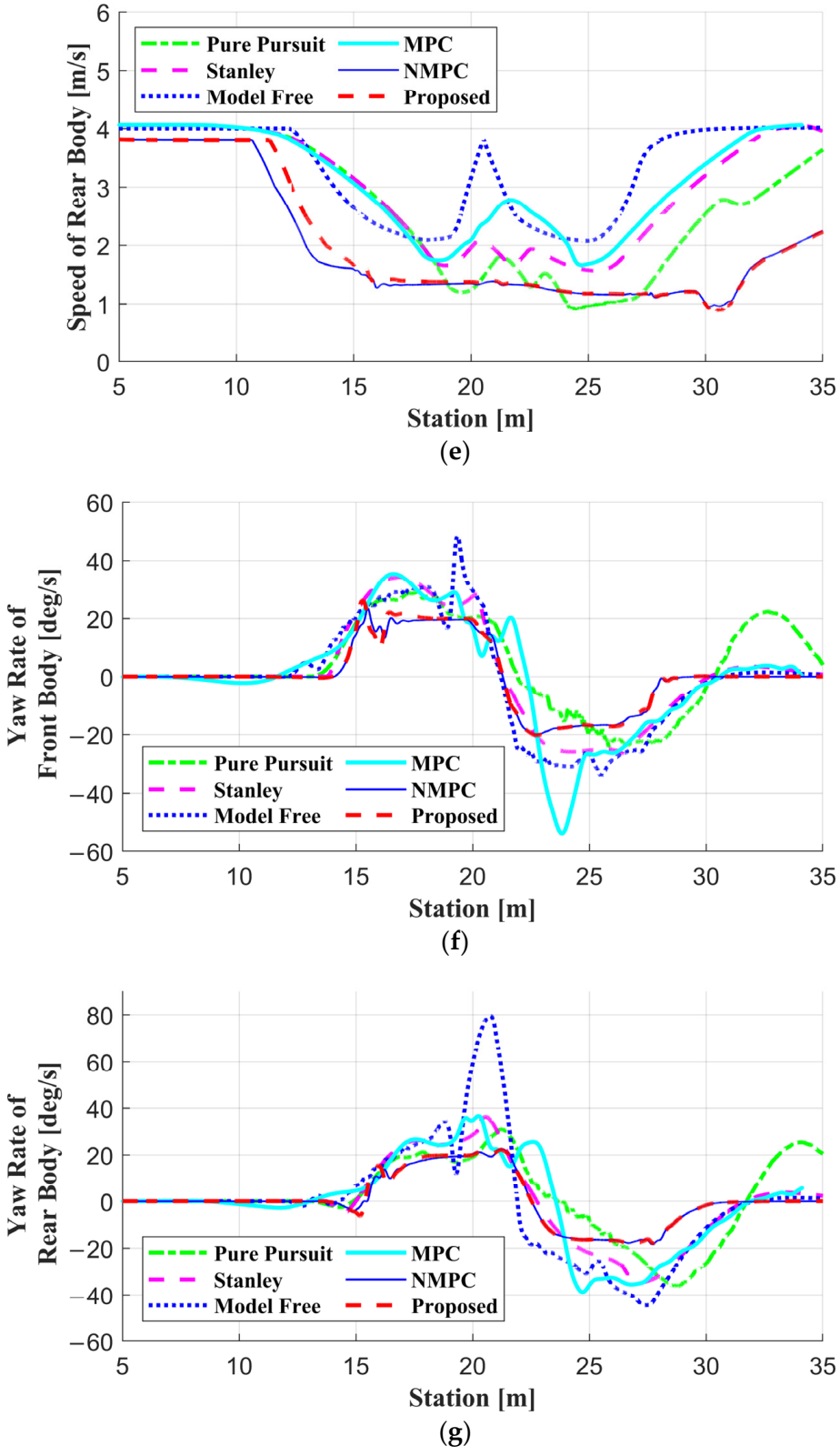

Figure 7. *Cont.*

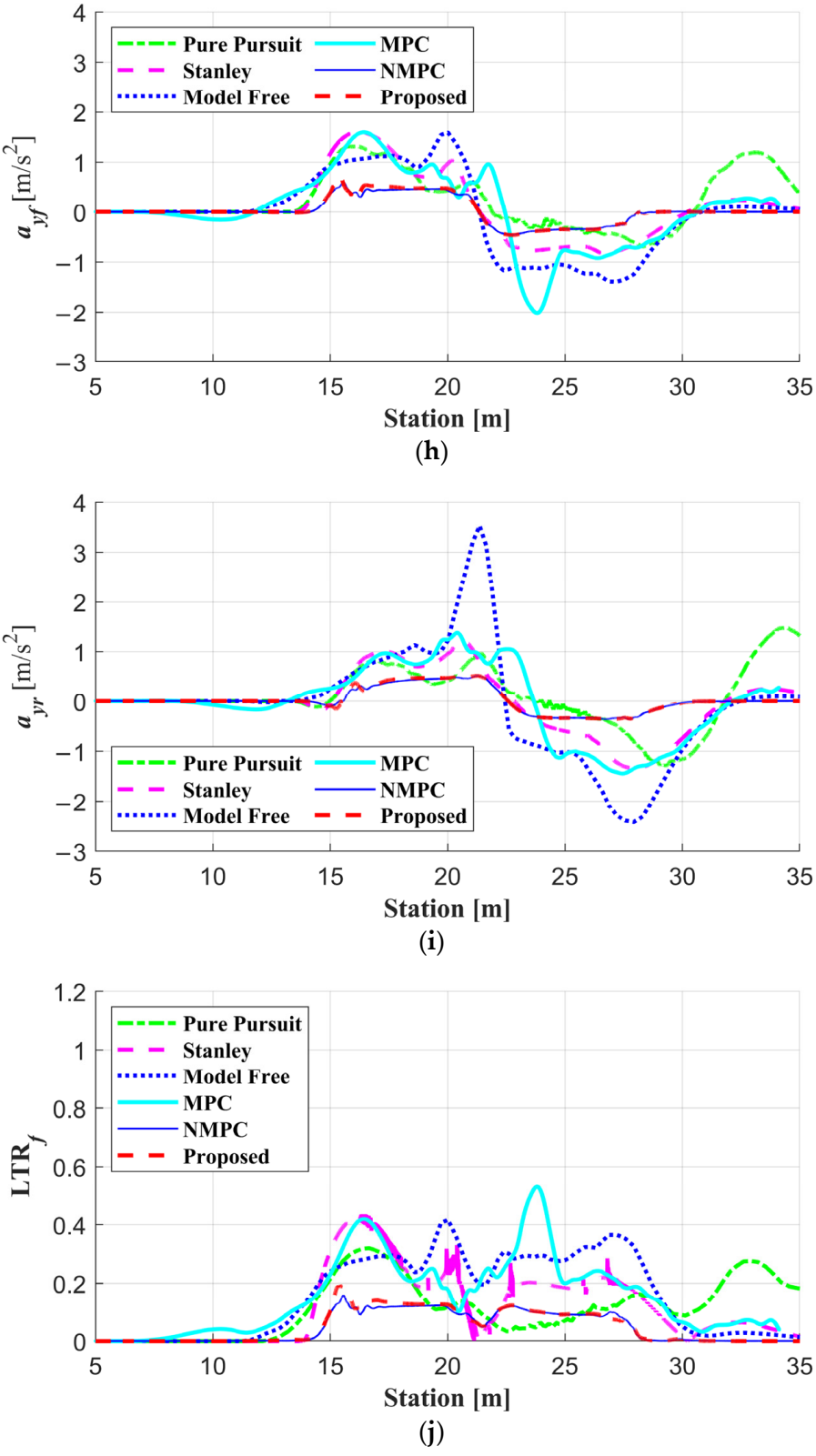

Figure 7. *Cont.*

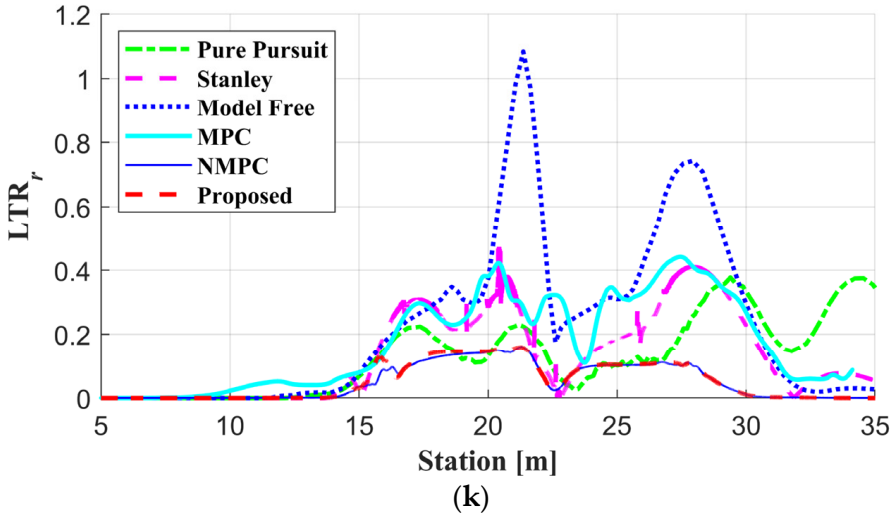

Figure 7. Simulation results of each algorithm: (**a**) lateral error, (**b**) heading angle error, (**c**) articulation angle, (**d**) speed of the front body, (**e**) speed of the rear body, (**f**) yaw rate of the front body, (**g**) yaw rate of the rear body, (**h**) lateral acceleration of the front body, (**i**) lateral acceleration of the rear body, (**j**) LTR of the front body, and (**k**) LTR of the rear body.

Table 2. Performance comparison between controllers.

Criteria	Pure Pursuit	Stanley	Model-Free	MPC	NMPC	Proposed
Mean (SD) of lateral error [m]	0.2426 (0.2116)	0.0461 (0.0593)	0.0722 (0.0797)	0.0553 (0.0576)	0.0126 (0.0123)	0.0118 (0.0121)
Max of lateral error [m]	0.6316	0.2096	0.2080	0.2787	0.0440	0.0421
Mean (SD) of heading error [deg]	6.1436 (5.9071)	1.5757 (2.3618)	1.8167 (3.1763)	2.2813 (3.0603)	1.0446 (1.8025)	1.0055 (1.7717)
Max of heading error [deg]	19.3495	12.6665	17.2790	14.2206	9.7883	9.5770
Max of a_y [m/s^2]	1.4818	1.6575	3.5317	1.5958	0.6046	0.7955
Max of LTR	0.3798	0.4734	1.0839	0.5300	0.1628	0.2210

The histories of the simulation results are depicted in Figure 7. Figure 7a,b shows the histories of the lateral and heading errors. The lateral and heading errors for the proposed algorithm are maintained below 0.05 m and 10 deg, respectively. Except for the inflection point at which the heading angle of the road changes in reverse, the heading error remains within 6 deg. NMPC shows almost the same errors as the proposed algorithm. As can be seen from Figure 7, the lateral and heading errors of the base algorithms increased by about two to five times compared to the proposed algorithm. The pure pursuit method showed the worst performance among the algorithms. The Stanley method shows a similar tracking performance to the proposed algorithm before passing the inflection point. However, lateral and heading errors increased at the inflection point and failed to decrease to a similar level at the first arc. The model-free method showed the largest overshoot of the heading error at the inflection point compared to other algorithms. This is because the model-free method models the behavior of the vehicle as a first-order delay model. Thus, the vehicle is assumed to be a point mass model. This means that the heading is explicitly considered in the steering angle decision. These characteristics resulted in a greater increase in heading error than the lateral one. The MPC without actuator delay showed a similar shape to the proposed algorithm, but the scale is enlarged by two times.

Figure 7c shows the history of the articulation angle. As shown in Figure 7c, the pure pursuit method generated the delayed control input, which caused a large deviation from the reference path. This phenomenon also occurred for the MPC algorithm. Meanwhile, the model-free method showed earlier steering than other methods, which caused the AAEV

to drive inside of the reference path, as shown in Figure 6. The Stanley method showed the most similar articulation angle history to the proposed algorithm and NMPC. The speed of the front and rear bodies are depicted in Figure 7d,e. Only the proposed algorithm and NMPC properly managed the speed of both bodies. Thus, the speed was reduced below the v_{set} before entering the arc to compensate for the actuation delay of the articulation and longitudinal actuator. It is worth noting that in the case of NMPC, the deceleration decision was made faster than the proposed algorithm due to the accurate vehicle model. Since the model-free approach selects the preview point to calculate the road curvature, the speed at the inflection point increases. The other methods reached a similar speed to the proposed algorithm after entering the arcs. The performance of the speed control affects the yaw rate and lateral acceleration of the AAEV. The histories of the yaw rate and lateral acceleration are described in Figure 7f,g and 7h,i, respectively. The lateral acceleration did not increase to a level at risk of rollover. However, the proposed algorithm and NMPC only satisfied the lateral acceleration threshold. Since the base algorithms are designed based on the front body, the increment of the lateral acceleration of the rear body is larger than that of the front body. In addition, the base algorithms without prediction, such as pure pursuit, Stanley, and model-free, are vulnerable to the change of the road curvature because the one waypoint on the reference path is considered to determine the desired inputs. The same trend is observed from the LTR_f and LTR_r as shown in Figure 7j,k. Particularly, the LTR_r of the AAEV governed by the model-free method exceeded one, which means that rollover occurred.

Table 2 summarized the key performance index (KPI) of the simulation study. As given in Table 2, the mean and SD of lateral error from the proposed algorithm and NMPC are smaller than 0.05 m. The maximum lateral error from the proposed algorithm is 0.0421 m, which is a negligible level for path tracking. For heading error, the mean and SD of the proposed algorithm are about 1 deg and the maximum is about 9.5 deg. In nominal driving conditions, the heading error of 9 deg is quite a large value. However, the reference path of the simulation study is a severe condition. Thus, the heading error of 9 deg is an acceptable level. Meanwhile, the base algorithms showed a larger mean, SD, and maximum lateral and heading errors. In addition, the maximum lateral acceleration exceeds at least 0.5 m/s^2 to 2.5 m/s^2. Similarly, the maximum LTR of base algorithms is 1.5 to four times larger than the proposed one. Thus, the proposed MPC-based integrated controller for the AAEV achieved the best performance of path tracking while preventing rollover by controlling the longitudinal motion. In particular, the proposed algorithm achieves performance equivalent to that of NMPC. As shown in Table 2, for KPI related to path tracking, the proposed algorithm and NMPC showed almost the same performance. However, the lateral acceleration and LTR of the NMPC are smaller than that of the proposed algorithm. Since the proposed algorithm satisfies all the constraints of MPC and prevents the rollover, the proposed algorithm is more appropriate in real-vehicle environments than in NMPC, considering the real-time performance. In particular, the average calculation times of the proposed algorithm and NMPC are about 40 ms and 200 ms, respectively. The sampling time of the NMPC is difficult to apply in a real-time environment. Therefore, the proposed algorithm improves path tracking and rollover prevention while securing real-time performance.

An additional simulation study was conducted to analyze the effect of the real-time application. Since the proposed algorithm is designed by using the linear MPC, the proposed algorithm has less computational burden than nonlinear MPC. When implemented with CVXGEN in a MATLAB/Simulink environment, the execution time of the proposed algorithm is within 40 ms. The simulation results with a sampling time of 10 ms and 40 ms are summarized in Figure 8. As shown in Figure 8a–h, the algorithm for both sampling times shows similar results. Since the control delay is considered in the MPC formulation, it is possible to prevent performance degradation due to the sampling time of the controller when applied in real time.

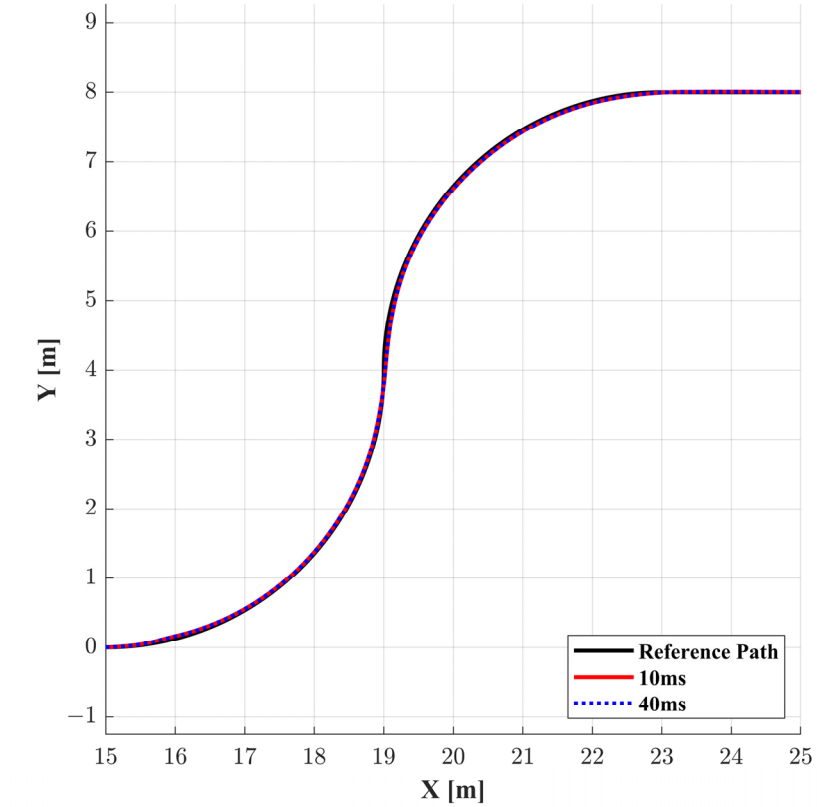

(**a**)

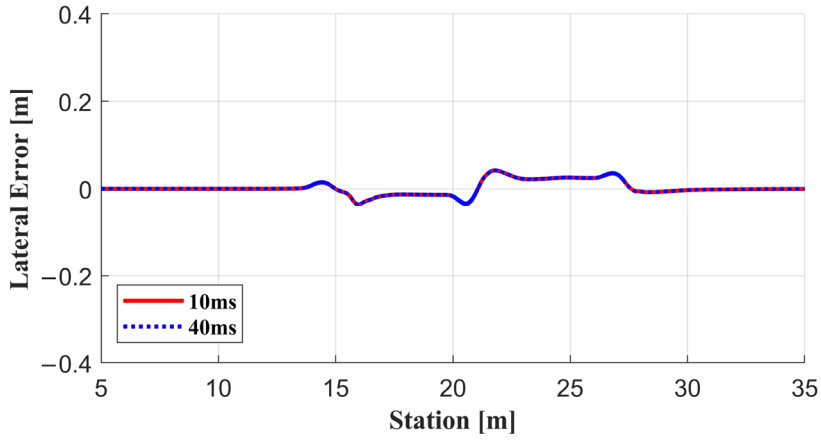

(**b**)

Figure 8. *Cont.*

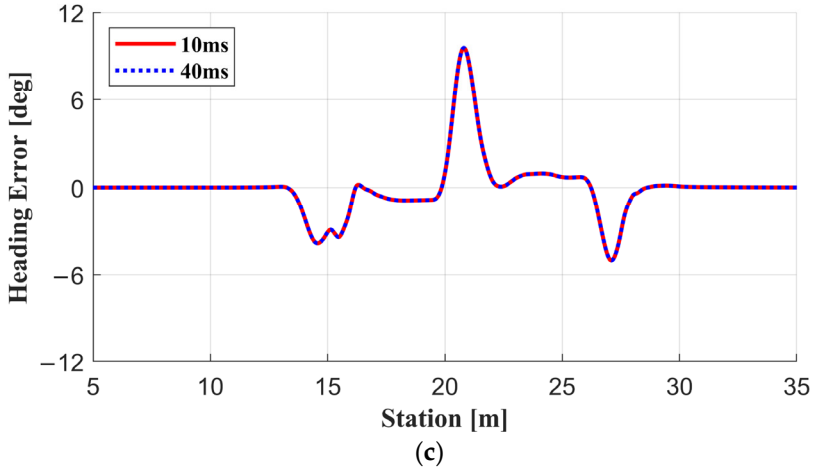

(c)

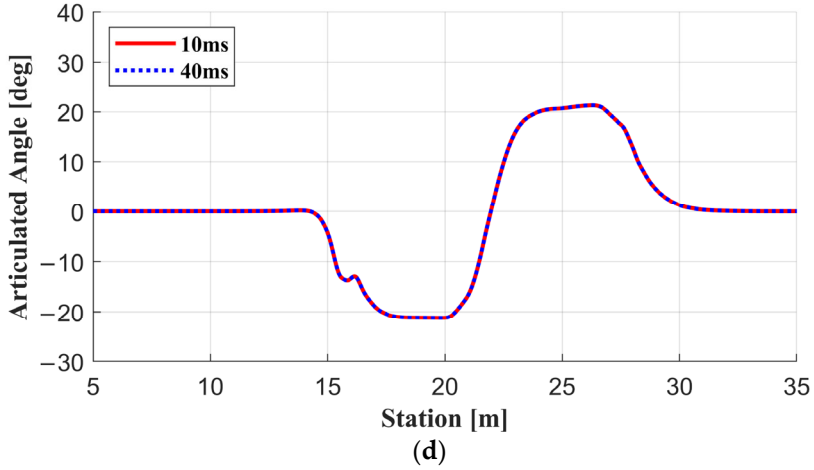

(d)

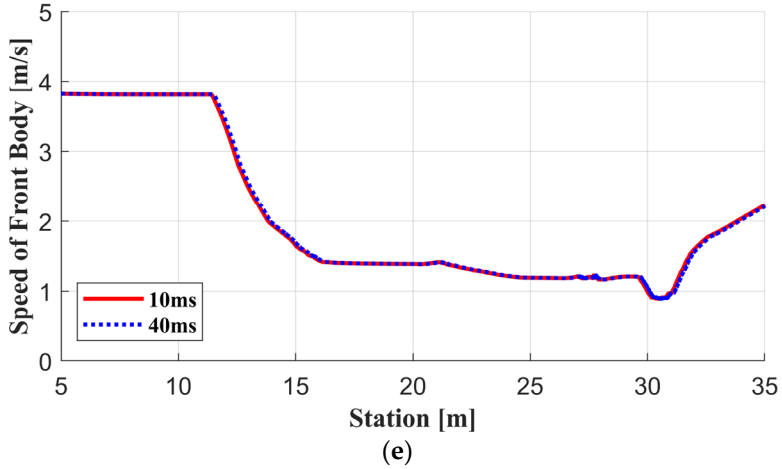

(e)

Figure 8. *Cont.*

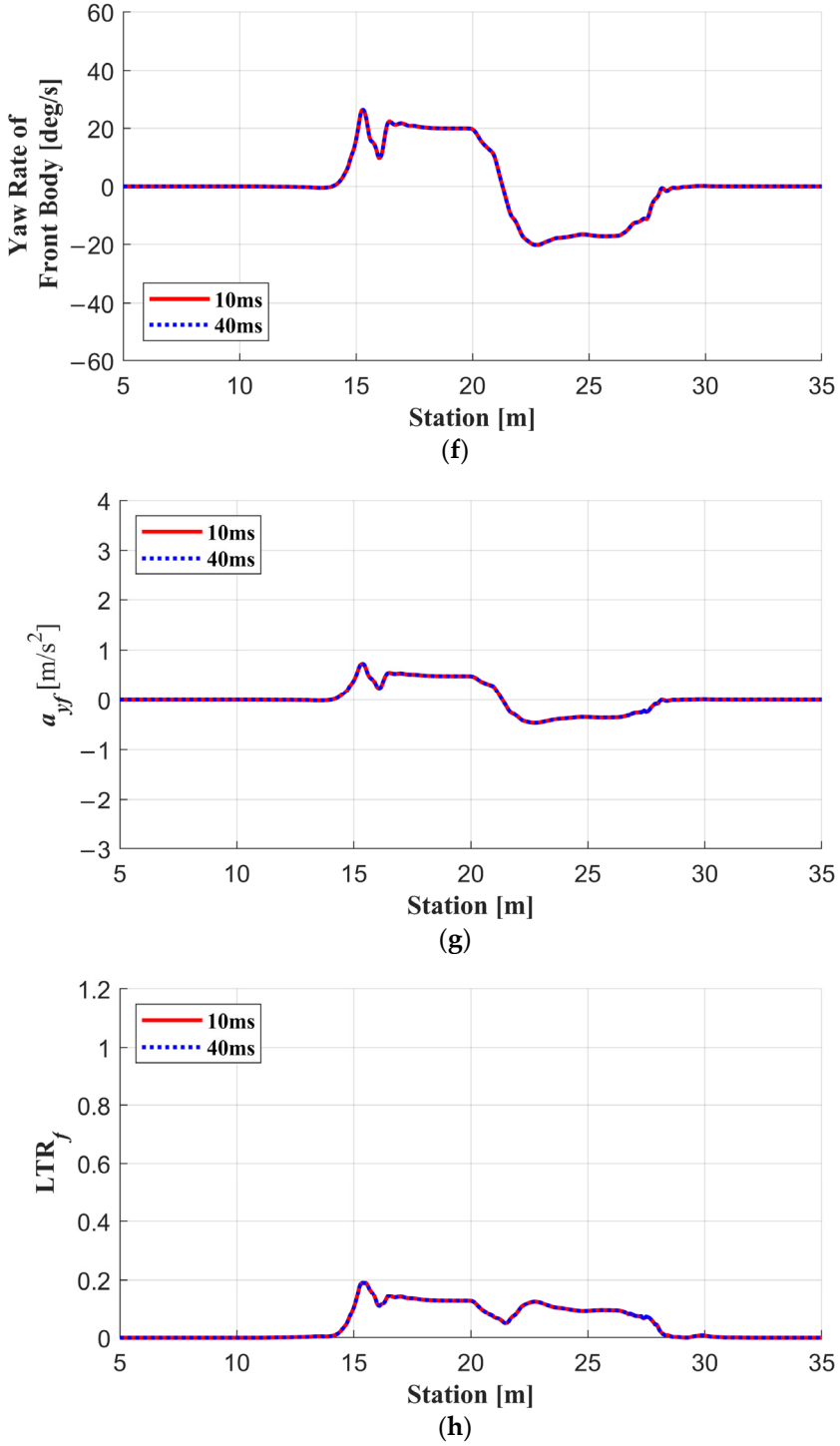

Figure 8. Simulation results of each algorithm: (**a**) driving trajectory, (**b**) lateral error, (**c**) heading angle error, (**d**) articulation Ile, (**e**) speed of the front body, (**f**) yaw rate of the front body, (**g**) lateral acceleration of the front body, and (**h**) LTR of the front body.

6. Conclusions

This paper presents the integrated controller for path tracking and velocity control with rollover prevention of the AAEV. To design the controller, a kinematic vehicle model is derived to represent the behavior of the AAEV. Since the AFS is generally used to generate the large yaw motion and smaller turning radius for narrow road conditions, the ODD is limited to low-speed driving conditions. Thus, the kinematic model is appropriate to model the behavior of the AAEV. The actuator delay is also considered to improve the

accuracy of the vehicle model. The proposed algorithm is composed of three submodules: reference state decision module, MPC-based reference state tracker, and low-level controller. The reference state decision module generates the reference position and heading angle of the front body. In addition, the maximum velocity to prevent the rollover is determined by considering the lateral behavior of both bodies. The MPC-based reference state tracker determines the desired articulation angle rate and longitudinal acceleration with the kinematic vehicle model, reference states, and constraints. The behavior relationship between the front and rear bodies is used to assign the velocity constraints for the rear body. The low-level controller converts the outputs from the MPC to actuator inputs to control the AAEV. The simulation study was conducted to evaluate the proposed algorithm and compare it with base algorithms. The proposed algorithm showed enhanced path tracking and velocity control.

Future works on the controller for the AAEV should address three aspects. The first aspect is to introduce the dynamic model to the vehicle controller. If the articulation angle is restricted within a small range, the ODD can be extended to the high-speed region. In this case, the dynamic model is required to model the behavior of the AAEV. The second aspect is to consider the steerable front wheel. Vehicles with front steering and an articulation joint have a degree of freedom to adjust the posture of the AAEV while following the target yaw rate. Thus, it is possible to pass through narrow or complex roads, thereby improving mobility. It is necessary to develop a controller which is designed for multiple actuators for the lateral motion of the AAEV. The final aspect is to implement and test the proposed algorithm on the real AAEV.

Funding: This study was financially supported by Seoul National University of Science & Technology.

Data Availability Statement: Not applicable.

Conflicts of Interest: The author declares no conflict of interest.

References

1. Hildenbrand, J. Developments in Heavy Construction Equipment. *Purdue Road Sch.* **1979**, *12*, 124–140.
2. Holm, I.C. Articulated, wheeled off-the-road vehicles. *J. Terramechanics* **1970**, *7*, 19–54. [CrossRef]
3. Dongtao, H.; Jinhao, L.; Jiangming, K.; Weiguo, T. Analysis of a Kinematic Model for a Forestry Six-Wheeled Luffing Articulated Vehicle Chassis. *Open J. Mech. Eng.* **2015**, *9*, 670–677. [CrossRef]
4. Polotski, V.; Hemami, A. Control of articulated vehicle for mining applications: Modeling and laboratory experiments. In Proceedings of the 1997 IEEE International Conference on Control Applications, Hartford, CT, USA, 5–7 October 1997.
5. Boulanger, A.G.; Chu, A.C.; Maxx, S.; Waltz, D.L. Vehicle electrification: Status and issues. *Proc. IEEE* **2011**, *99*, 1116–1138. [CrossRef]
6. Monteiro, V.; Afonso, J.A.; Ferreira, J.C.; Afonso, J.L. Vehicle electrification: New challenges and opportunities for smart grids. *Energies* **2018**, *12*, 118. [CrossRef]
7. Chen, F.; Taylor, N.; Kringos, N. Electrification of roads: Opportunities and challenges. *Appl. Energy* **2015**, *150*, 109–119. [CrossRef]
8. 8Fast Facts U.S. Transportation Sector GHG Emissions. Available online: https://www.epa.gov/greenvehicles/archives-fast-facts-us-transportation-sector-greenhouse-gas-emissions (accessed on 26 September 2022).
9. Prassler, E.; Ritter, A.; Schaeffer, C.; Fiorini, P. A short history of cleaning robots. *Auton. Robots* **2000**, *9*, 211–226. [CrossRef]
10. Prassler, E.; Schwammkrug, D.; Rohrmoser, B.; Schmidl, G. A robotic road sweeper. In Proceedings of the 2000 ICRA Millennium Conference IEEE International Conference on Robotics and Automation, Symposia Proceedings, San Francisco, CA, USA, 24–28 April 2000.
11. Yin, X.; Zhu, L. Structure Design and Kinematics Analysis for a New-type All-electric Sweeper. In Proceedings of the 2015 3rd International Conference on Mechanical Engineering and Intelligent Systems, Yinchuan, China, 15–16 August 2015.
12. Jeon, J.; Jung, B.; Koo, J.C.; Choi, H.R.; Moon, H.; Pintado, A.; Oh, P. Autonomous robotic street sweeping: Initial attempt for curbside sweeping. In Proceedings of the 2017 IEEE International Conference on Consumer Electronics (ICCE), Las Vegas, NV, USA, 8–10 January 2017.
13. Lei, T.; Wang, J.; Yao, Z. Modelling and stability analysis of articulated vehicles. *Appl. Sci.* **2021**, *11*, 3663. [CrossRef]
14. He, Y.; Khajepour, A.; McPhee, J.; Wang, X. Dynamic modelling and stability analysis of articulated frame steer vehicles. *Int. J. Heavy Veh. Syst.* **2005**, *12*, 28–59. [CrossRef]
15. Michałek, M.M.; Patkowski, B.; Gawron, T. Modular kinematic modelling of articulated buses. *IEEE Trans. Veh. Technol.* **2020**, *69*, 8381–8394. [CrossRef]

16. Sun, T.; He, Y. *Phase-Plane Analysis for Evaluating the Lateral Stability of Articulated Vehicles*; SAE Technical Paper; No. 2015-01-1574; SAE: Pittsburgh, PA, USA, 2015.
17. Van de Molengraft-Luijten, M.F.J.; Besselink, I.J.; Verschuren, R.M.A.F.; Nijmeijer, H. Analysis of the lateral dynamic behaviour of articulated commercial vehicles. *Veh. Syst. Dyn.* **2012**, *50*, 169–189. [CrossRef]
18. Bao, J.-H.; Li, J.-L.; Yan, Y. Lateral stability analysis of the tractor/full trailer combination vehicle. In Proceedings of the 2011 International Conference on Electric Information and Control Engineering, Wuhan, China, 15–17 April 2011.
19. Sharifzadeh, M.; Farnam, A.; Senatore, A.; Timpone, F.; Akbari, A. Delay-dependent criteria for robust dynamic stability control of articulated vehicles. In Proceedings of the International Conference on Robotics in Alpe-Adria Danube Region, Torino, Italy, 21–23 June 2017.
20. Azad, N.L.; McPhee, J.; Khajepour, A. Off-road lateral stability analysis of an articulated steer vehicle with a rear-mounted load. *Int. J. Veh. Syst. Model. Test.* **2005**, *1*, 106–130. [CrossRef]
21. Wang, B.; Zha, H.; Zhong, G.; Li, Q.; Wang, X. Integrated active steering control strategy for autonomous articulated vehicles. *Int. J. Heavy Veh. Syst.* **2020**, *27*, 565–599. [CrossRef]
22. Zhang, Y.; Khajepour, A.; Ataei, M. A universal and reconfigurable stability control methodology for articulated vehicles with any configurations. *IEEE Trans. Veh. Technol.* **2020**, *69*, 3748–3759. [CrossRef]
23. Zhang, Y.; Khajepour, A.; Hashemi, E.; Qin, Y.; Huang, Y. Reconfigurable model predictive control for articulated vehicle stability with experimental validation. *IEEE Trans. Transp. Electrif.* **2020**, *6*, 308–317. [CrossRef]
24. Wang, W.; Fan, J.; Xiong, R.; Sun, F. Lateral stability control of four wheels independently drive articulated electric vehicle. In Proceedings of the 2016 IEEE Transportation Electrification Conference and Expo (ITEC), Dearborn, MI, USA, 27–29 June 2016.
25. Sahin, H.; Akalin, O. Articulated Vehicle Lateral Stability Management via Active Rear-Wheel Steering of Tractor Using Fuzzy Logic and Model Predictive Control. *SAE Int. J. Commer. Veh.* **2020**, *13*, 115–129. [CrossRef]
26. Rehnberg, A.; Drugge, L.; Stensson Trigell, A. Snaking stability of articulated frame steer vehicles with axle suspension. *Int. J. Heavy Veh. Syst.* **2010**, *17*, 119–138. [CrossRef]
27. Esmaeili, N.; Kazemi, R.; Tabatabaei Oreh, S.H. An adaptive sliding mode controller for the lateral control of articulated long vehicles. *Proc. Inst. Mech. Eng. K J. Multi-Body Dyn.* **2019**, *233*, 487–515. [CrossRef]
28. Saeedi, M.A. A new effective nonlinear strategy for lateral stability increment of an articulated vehicle rigid cargo. *Proc. Inst. Mech. Eng. D J. Automob. Eng.* **2021**, *in press*. [CrossRef]
29. Saeedi, M.A.; Kazemi, R.; Azadi, S. A new robust controller to improve the lateral dynamic of an articulated vehicle carrying liquid. *Proc. Inst. Mech. Eng. K J. Multi-Body Dyn.* **2017**, *231*, 295–315. [CrossRef]
30. Badue, C.; Guidolini, R.; Carneiro, R.V.; Azevedo, P.; Cardoso, V.B.; Forechi, A.; Jesus, L.; Berriel, R.; Paixão, T.; Mutz, F.; et al. Self-driving cars: A survey. *Expert Syst. Appl.* **2021**, *165*, 113816. [CrossRef]
31. Tian, J.; Zeng, Q.; Wang, P.; Wang, X. Active steering control based on preview theory for articulated heavy vehicles. *PLoS ONE* **2021**, *16*, e0252098. [CrossRef] [PubMed]
32. Jujnovich, B.A.; Cebon, D. Path-following steering control for articulated vehicles. *J. Dyn. Syst. Meas. Control* **2013**, *135*, 031006. [CrossRef]
33. De Bruin, D.; Damen, A.A.H.; Pogromsky, A.; Van Den Bosch, P.P.J. Backstepping control for lateral guidance of all-wheel steered multiple articulated vehicles. In Proceedings of the ITSC2000. 2000 IEEE Intelligent Transportation Systems. Proceedings, Dearborn, MI, USA, 1–3 October 2000.
34. Felez, J.; GarcíA-Sanchez, C.; Lozano, J.A. Control design for an articulated truck with autonomous driving in an electrified highway. *IEEE Access* **2018**, *6*, 60171–60186. [CrossRef]
35. Dou, F.; Huang, Y.; Liu, L.; Wang, H.; Meng, Y.; Zhao, L. Path planning and tracking for autonomous mining articulated vehicles. *Int. J. Heavy Veh. Syst.* **2019**, *26*, 315–333. [CrossRef]
36. Guan, H.; Kim, K.; Wang, B. Comprehensive path and attitude control of articulated vehicles for varying vehicle conditions. *Int. J. Heavy Veh. Syst.* **2017**, *24*, 65–95. [CrossRef]
37. Tan, S.; Zhao, X.; Yang, J.; Zhang, W. A path tracking algorithm for articulated vehicle: Development and simulations. In Proceedings of the 2017 IEEE Transportation Electrification Conference and Expo, Asia-Pacific (ITEC Asia-Pacific), Harbin, China, 7–10 August 2017.
38. Yao, D.; Xie, H.; Qiang, W.; Liu, Y.; Xiong, S. Accurate trajectory tracking with disturbance-resistant and heading estimation method for self-driving vibratory roller. *IFAC-Pap.* **2018**, *51*, 754–758. [CrossRef]
39. Dou, F.; Liu, W.; Huang, Y.; Liu, L.; Meng, Y. Modeling and path tracking for articulated steering vehicles. In Proceedings of the 2017 Chinese Automation Congress (CAC), Jinan, China, 20–22 October 2017.
40. Shi, G.; Yang, J.; Zhao, X.; Li, Y.; Zhao, Y.; Li, J. A-infinity control for path tracking with fuzzy hyperbolic tangent model. *J. Control Sci. Eng.* **2016**, *2016*, 9072831. [CrossRef]
41. Wei, K.; Liu, X.; Wei, C.; Feng, R. Path Tracking Control of the Wheeled off-road Articulated Vehicle with Actuator Saturation. *Metall. Min. Ind.* **2013**, *9*, 1024–1029.
42. Zhao, X.; Yang, J.; Zhang, W.; Zeng, J. Feedback linearization control for path tracking of articulated dump truck. *Telkomnika* **2015**, *13*, 922–929. [CrossRef]
43. Nayl, T.; Nikolakopoulos, G.; Gustfsson, T. Switching model predictive control for an articulated vehicle under varying slip angle. In Proceedings of the 2012 20th Mediterranean Conference on Control & Automation (MED), Barcelona, Spain, 3–6 July 2021.

44. Nayl, T.; Nikolakopoulos, G.; Gustafsson, T. A full error dynamics switching modeling and control scheme for an articulated vehicle. *Int. J. Control Autom. Syst.* **2015**, *13*, 1221–1232. [CrossRef]
45. Bai, G.; Meng, Y.; Liu, L.; Luo, W.; Gu, Q.; Li, K. A new path tracking method based on multilayer model predictive control. *Appl. Sci.* **2019**, *9*, 2649. [CrossRef]
46. Bai, G.; Liu, L.; Meng, Y.; Luo, W.; Gu, Q.; Ma, B. Path tracking of mining vehicles based on nonlinear model predictive control. *Appl. Sci.* **2019**, *9*, 1372. [CrossRef]
47. Jeong, Y.; Kim, W.; Yim, S. Model Predictive Control Based Path Tracking and Velocity Control with Rollover Prevention Function for Autonomous Electric Road Sweeper. *Energies* **2022**, *15*, 984. [CrossRef]
48. Nayl, T.; Nikolakopoulos, G.; Gustafsson, T. Effect of kinematic parameters on MPC based on-line motion planning for an articulated vehicle. *Robot. Auton. Syst.* **2015**, *70*, 16–24. [CrossRef]
49. Jung, C.; Kim, H.; Son, Y.; Lee, K.; Yi, K. Parameter adaptive steering control for autonomous driving. In Proceedings of the 17th International IEEE Conference on Intelligent Transportation Systems (ITSC), Qingdao, China, 8–11 October 2014.
50. Yoon, J.; Kim, D.; Yi, K. Design of a rollover index-based vehicle stability control scheme. *Veh. Syst. Dyn.* **2007**, *45*, 459–475. [CrossRef]
51. Yoon, J.; Yim, S.; Cho, W.; Koo, B.; Yi, K. Design of an unified chassis controller for rollover prevention, manoeuvrability and lateral stability. *Veh. Syst. Dyn.* **2010**, *48*, 1247–1268. [CrossRef]
52. Zeilinger, M.N.; Jones, C.N.; Morari, M. Robust stability properties of soft constrained MPC. In Proceedings of the 49th IEEE Conference on Decision and Control (CDC), Atlanta, GA, USA, 15–17 December 2010.
53. Mattingley, J.; Boyd, S. CVXGEN: A code generator for embedded convex optimization. *Optim. Eng.* **2021**, *13*, 1–27. [CrossRef]
54. Coulter, R.C. *Implementation of the Pure Pursuit Path Tracking Algorithm*; ADA255524; Carnegie-Mellon UNIV Pittsburgh PA Robotics INST: Pittsburgh, PA, USA, 1992.
55. Thrun, S.; Montemerlo, M.; Dahlkamp, H.; Stavens, D.; Aron, A.; Diebel, J.; Fong, P.; Gale, J.; Halpenny, M.; Hoffmann, G.; et al. Stanley: The robot that won the DARPA Grand Challenge. *J. Field Robot.* **2006**, *23*, 661–692. [CrossRef]
56. Andersson, J.A.; Gillis, J.; Horn, G.; Rawlings, J.B.; Diehl, M. CasADi: A software framework for nonlinear optimization and optimal control. *Math. Program. Comput.* **2019**, *11*, 1–36. [CrossRef]